Tetrahedron 68 (2012) 1704–1711

Contents lists available at SciVerse ScienceDirect

Tetrahedron

journal homepage: www.elsevier.com/locate/tet

N,*N*-Dimethylaniline and 1-(trifluoromethyl)benzene-functionalized tetrakis(ethynyl)pyrenes: synthesis, photophysical, electrochemical and computational studies

Yeon Ok Lee [a,†], Tuhin Pradhan [a,†], Kwanghyun No [b,*], Jong Seung Kim [a,*]

[a] *Department of Chemistry, Korea University, Seoul 136-701, Republic of Korea*
[b] *Department of Chemistry, Sookmyung Women's University, Seoul 140-742, Republic of Korea*

ARTICLE INFO

Article history:
Received 16 November 2011
Received in revised form 21 December 2011
Accepted 21 December 2011
Available online 27 December 2011

Keywords:
Tetrakis(phenylethynyl)pyrene
Substitution pattern
Radical stability
DFT calculation

ABSTRACT

We have synthesized a series of tetrakis(ethynyl)pyrenes functionalized with *N*,*N*-dimethyaniline and 1-(trifluoromethyl)benzene as a peripheral electron-donor and electron-acceptor moiety, respectively. In solvatochromic studies, compounds with one peripheral donor and three peripheral acceptors (**2**), with two donors and two acceptors (**3** and **4**), with three donors and one acceptor (**5**) show enhanced charge transfer compared with tetra-donor (**6**) and tetra-acceptor (**1**) compounds. The redox peak reversibility depends on the number of peripheral donors and acceptors appended to tetrakis(ethynyl)pyrenes as well as on their substitution pattern as revealed by cyclic voltammetric studies. The photophysical and electrochemical properties of compounds **1**–**5** have been compared with compound (**6**) reported recently by J.-W. Oh et al. [*Angew. Chem., Int. Ed.* **2009**, *48*, 2522–2524]. The density functional theory (DFT) based calculations such as spin density distribution (SDD) of cation/anion radicals, electrostatic potential (ESP) density distribution, non-adiabatic reduction potentials (NRP) for cation radicals, and vertical detachment energy (VDE) for anion radicals supported the experimental observations. The differences in oxidation peak reversibility for different substitution pattern have been rationalized by calculated static first hyperpolarizability (β). Our observations would be helpful in designing new ECL-active materials, where ECL (electrogenerated chemiluminescence) efficiency can be improved through improving radical stability.

1. Introduction

Pyrene is a polycyclic aromatic hydrocarbon (PAH).[1] Pyrene-based organic materials have been used for many purposes, especially for molecular electronic devices such as organic light emitting diodes (OLEDs),[2] electronic skin, etc. The fluorescence properties of pyrene have made its derivatives suitable to be used as biological probes for the investigation of structural properties of proteins and peptides,[3] DNA recognition,[4] surfactant micelles and vesicles properties.[5] Both photophysical and electronic properties of pyrenes have been exploited in optoelectronic devices such as organic photovoltaic cells (OPV),[6] organic field-effect transistors (OFETs),[7] organic lasers, solar cells, etc. More recently, authors have used the cruciform-type[8] structure of alkynylpyrene with peripheral multidonors substitution to prepare very efficient electrogenerated chemiluminescence (ECL) materials.[9a] The key of these versatile applications of pyrene derivatives is based on the way of multifold tuning of structure–property relationships. Subtle changes in structure can greatly alter not only the physical properties like solubility and stability in ambient air, but also the optical and electronic properties such as energy gap, electron affinity and electron transfer efficiency; even stability of cation or anion produced after electron donation or acceptance depends on structural changes at the molecular level.[10] The electrochemically generated cation and anion radical stabilities at the vicinity of electrode are very important criteria for showing ECL, which is a light emission from the excited-state molecules during electrochemical reactions.[9–11] There are very few examples[9a,10] of improving radical stability for improving ECL efficiency. Bard et al.[10a] have improved the stability of oxidized fluorene compound for ECL by modifying the fluorene ring to 9,9′-spirobifluorene derivatives. Although pyrene derivatives are well known for their poor ECL properties because of the instability of cations produced electrochemically, we observed, in our previous work,[9a] that ECL efficiencies of the pyrene derivatives increase proportionally with the number of peripheral donors, which correspond to their improved cation radical stability. There is no report of using peripheral acceptors appended to

* Corresponding authors. E-mail addresses: hyun@sookmyung.ac.kr (K. No), jongskim@korea.ac.kr (J.S. Kim).
† Equally contributed to this work.

0040-4020/$ – see front matter © 2012 Elsevier Ltd. All rights reserved.
doi:10.1016/j.tet.2011.12.066

alkynylpyrene unit for investigating cation or/and anion radical stability for ECL.

In this present work, we have prepared a series of alkynylpyrene derivatives (Scheme 1), where pyrene acts as central acceptor moiety,[9] *N*,*N*-dimethylaniline and 1-(trifluoromethyl)benzene act, respectively, as peripheral donor and peripheral acceptor moieties. An ethynyl group acts as a bridge between central acceptor and peripheral donor (D-π-cA, cA=central acceptor) and between central acceptor and peripheral acceptor (cA-π-A) as well. The reason of using peripheral acceptor is that it may communicate with peripheral donor through central acceptor, which can extend the electronic conjugation for intramolecular charge transfer (ICT).[10b,11a,12] We have varied the number of peripheral donor and acceptor groups appended to alkynylpyrene unit keeping the total number of peripheral donor and acceptor groups fixed, as to monitor the electrochemically produced radical stability. Keeping this in mind, we have also changed the substitution pattern of the peripheral donor and acceptor groups where the number of peripheral acceptors (or donors) is same. While the reported cruciform systems contain either peripheral donor or acceptor arms[9a,b] only, the present systems contain both peripheral donor and acceptor arms. We then studied photophysical and electrochemical properties of the synthesized compounds and compared them with a standard compound of similar kind, which is already reported in the literature.[9a] Finally, we have explained the observed cationic and/or anionic radical stability at the molecular level by density functional theory (DFT) based theoretical calculations.

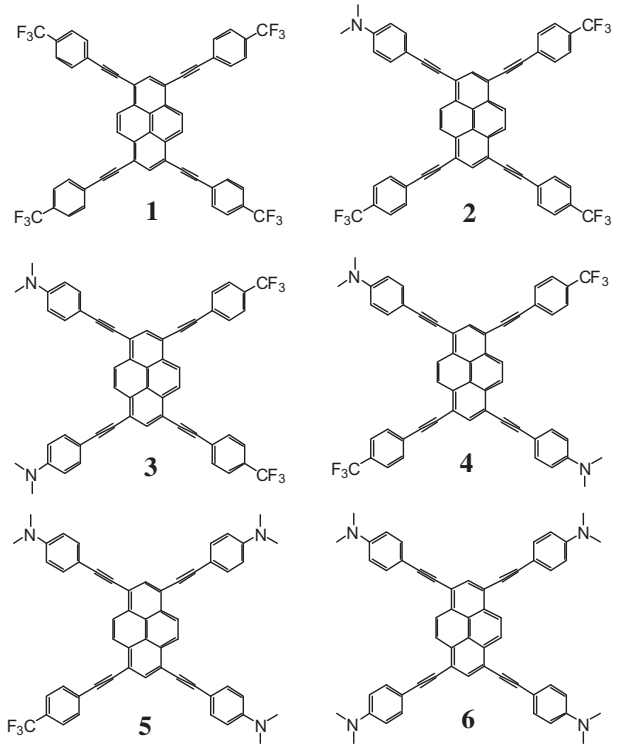

Scheme 1. Schematic molecular structures of **1**–**6**.

2. Results and discussion

The synthetic route for preparation of a series of **2**–**5** is depicted in Scheme 2. Compounds **1** and **6** were prepared by adaptation of procedures reported earlier.[13] Sonogashira cross-coupling of 1,3,6,8-tetrabromopyrene with 4-ethynyl-*N*,*N*-dimethylaniline gave a mixture of **7**–**10**, which were able to be isolated as pure compounds by silica mediated column chromatography. Compounds **2**–**5** were obtained by Sonogashira coupling of **7**–**10** with 4-ethynyl-benzotrifluoride.

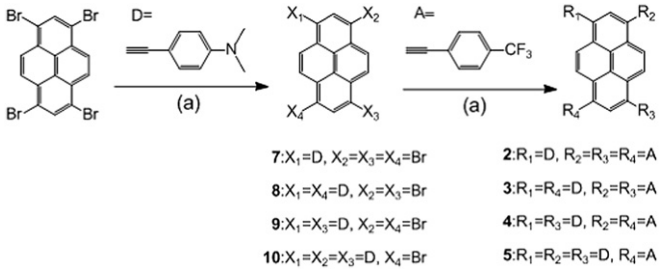

Scheme 2. Synthesis of **2**–**5**. Reagents and conditions: (a) $PdCl_2(PPh_3)_2$, CuI, PPh_3, Et_3N, toluene, 100 °C, 2 h.

We investigated the optical properties of **1**–**6**, and their selected spectroscopic data are shown in Fig. 1 and summarized in Table 1. The absorption of **1** peaked at 467 nm; however, this is bathochromically shifted by 34–42 nm when any electron withdrawing group (−CF_3) is replaced by an electron donating group (−NMe_2) in **2**, implying that the HOMO–LUMO gap in the molecule is decreased due to the increased conjugation length from the peripheral donor (*N*,*N*-dimethyl aniline) to the peripheral acceptor (1-(trifluoromethyl)benzene) moiety. It is noted that replacement of two or more acceptor groups in **1** with donor groups does not make a considerable change to the absorption peak position relative to that of **2**. Compounds **3** and **4** having same number of donor and acceptor groups did not show significant differences in peak position of the lowest-energy absorption band. In comparison to the absorption spectra, emission spectra show some significant spectral shifts depending on the number of acceptor and donor moieties in the tetrakis(ethynyl)pyrenes. This may be related to the excited-state dipole moment of the molecule as well as the solvent polarity. Among **1**–**6**, compound **2** shows the largest Stokes shift (steady state) in dichloromethane, and **1** shows the smallest. If the Stokes shifts for **1**–**6** are measured in same solvent (meaning that the solvent polarization function in the Lippert–Mataga equation[14] would be the same for **1**–**6**), according to the Lippert–Mataga relation, experimentally observed Stokes shift order: **2**>**3**≈**4**>**5**>**6**>**1** should follow the differences between ground- and excited-state dipole moments ($\Delta\mu$) for the six compounds. The value of $\Delta\mu$, in a D-π-cA-π-A system depends on how intramolecular charge transfer (ICT)[10b,12] occurs from peripheral donor to peripheral acceptor units.

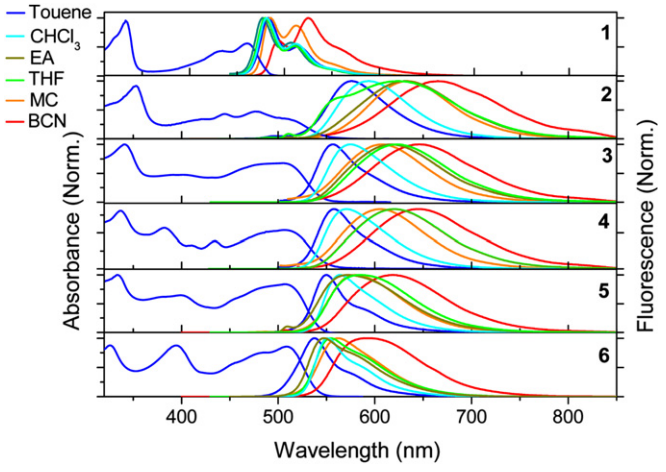

Fig. 1. Steady-state absorption and fluorescence spectra of **2**–**6** in various solvents.

Table 1
Parameters obtained from optical studies for **1**–**6**

Compd	λ_{max}^{abs} [nm][a]	$\lambda_{max}^{em.}$ [nm]	Stokes shift [cm^{-1}]	Φ[b]
1	467	491	1047	0.98
2	501	627	4011	0.43
3	506	608	3315	0.42
4	509	605	3117	0.45
5	506	576	2401	0.65
6	508	562	1891	0.60

[a] Recorded at the lowest-energy wavelengths.
[b] Using Rhodamine 6G in CH_2Cl_2. Φ_f=0.95 in EtOH. The photophysical data were obtained in CH_2Cl_2.

From this viewpoint, we may predict that **2**, with one peripheral donor and three peripheral acceptor arms, is the best compound with the most ICT. Compound **5** with three peripheral donors and one peripheral acceptor has weaker ICT than **2**. Given the two or three peripheral donor moieties in a molecule, the effect of electronic delocalization due to cross-conjugation between the peripheral donor moieties is expected to be significant. This may be a reason for the weaker ICT in **5** in comparison with **2**. Another possibility can also be discussed in this regard. *N*,*N*-Dimethyl aniline unit is known as a stronger electron-donor while 1-(trifluoromethyl)benzene unit is known as an weaker acceptor. Therefore, adding more than one peripheral donor has little further effect in **5**, whereas in **2**, three weaker acceptors plus the pyrene system (which is also a weaker acceptor) translates into a relatively strong acceptor, that is coupled to a strong NMe_2 donor. Another notable finding is that the ICT in **6** (D-π-cA system) is stronger than in **1** (A-π-cA system). The quantum yields for fluorescence, measured relative to Rhodamine 6G in ethanol as a standard,[15] were also determined for **1**–**6** in CH_2Cl_2 solution and given in Table 1. All the compounds have high quantum yields, which is a requirement for the compounds to be used as ECL-active materials.

The electrochemical behaviours of **2**–**6** were investigated by cyclic voltammetry (CV) with Bu_4NPF_6 in CH_2Cl_2 (0.1 M) on a Pt electrode as summarized in Fig. 2 and Table 2. Oxidation peaks of **2**–**6**, which may originate from the removal of one electron from the amino segment in peripheral donor groups, appear at 0.12–0.32 V. Easier oxidations are observed with increasing number of peripheral donor groups appended to the tetrakis(ethynyl)pyrenes. In comparison with **2** (one peripheral donor group), oxidation peak of **6** (four peripheral donor groups) is

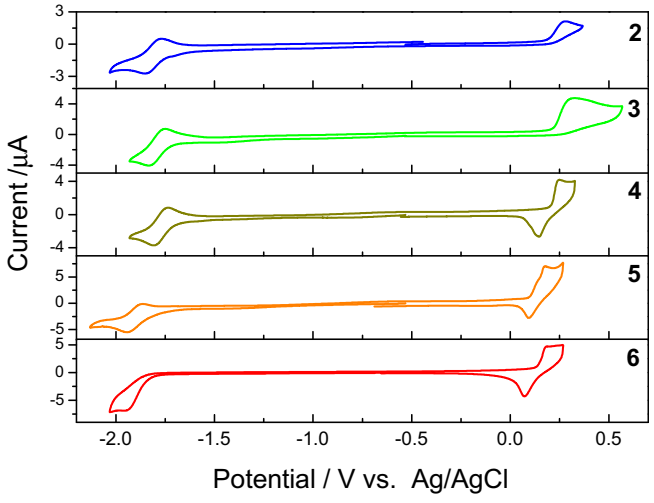

Fig. 2. Cyclic voltammograms of **2**–**6** (0.5 mM) for a Pt electrode with Bu_4NPF_6 in CH_2Cl_2 (0.1 M). Scan rate=100 mV s^{-1}.

Table 2
Parameters obtained from electrochemical, optical and theoretical studies for **1**–**6**

Compd	E_{pc} [V]	E_{pa} [V]	ΔE_{gap}^{elec} [eV][a]	ΔE_{gap}^{opt} [eV][b]	ΔE_{gap}^{calcd} [eV][c]	HOMO (eV) (calcd)	LUMO (eV) (calcd)
1	—	—	—	2.65	2.50	−5.44	−2.94
2	−1.81	0.28	2.09	2.47	2.32	−4.97	−2.66
3	−1.79	0.32	2.11	2.45	2.23	−4.65	−2.42
4	−1.76	0.24	2.10	2.43	2.28	−4.67	−2.38
5	−1.90	0.13	2.03	2.45	2.32	−4.42	−2.10
6	−1.95	0.12	2.07	2.44	2.37	−4.18	−1.80

[a] Electrochemical band gap calculated from the difference between the two redox peak potentials.
[b] HOMO–LUMO gap calculated from the lowest-energy UV–visible absorption band maximum in CH_2Cl_2.
[c] HOMO–LUMO gap calculated by DFT method at B3LYP/6-31G(d) level of theory. The photophysical and electrochemical data were obtained in CH_2Cl_2.

cathodically shifted by ~200 mV. In addition, the reversibility of the oxidation peak increases with the number of peripheral donor groups, indicating enhanced cation radical stability. Despite the fact that **3** and **4** have same number of donor and acceptor groups, they have different oxidation peak positions and reversibility, implying, respectively, different ease of oxidation and different cation radical stability (**3** and **4** exhibit oxidation peaks, respectively, at 0.32 and 0.24 V; **4** exhibits better reversibility). Compounds **2**–**5** displayed reversible reduction peaks located at −1.76 to −1.95 V. The reduction potential follows an opposite trend to the potential, in which the more difficult reductions are observed with increasing number of donor groups (**2**→**6**). In addition, reversibility of the reduction peaks diminished with increasing donor groups. This means that anion radical stability decreases with increasing number of donor groups (**2**→**6**). In other words, anion radical stability increases with increasing number of acceptor groups (**6**→**2**). However, compounds (**2**–**4**) having one or two donor groups (conversely with three or two acceptor groups, respectively) do not exhibit much change both in reversibility and reduction potential. From the perspective of both cation and anion radical stability, **4** and **5** are better candidates than the others (even than **6**),[9a] which may make them eligible for ECL applications.

To get insight into radical stabilities at the molecular level, computational studies were performed on compounds **1**–**6** by using density functional theory (DFT) at B3LYP/6-31G(d) level of theory in a suite of Gaussian 09 W programs.[16] The HOMO (highest occupied molecular orbital) energy level raises on going from **1** to **6** (Table 2). This is consistent with literature reports for D-π-A system, where HOMO energy level raised upon introduction of donor groups.[10b] Interestingly, LUMO (lowest unoccupied molecular orbital) energy level also follows the same trend (Table 2). The HOMO–LUMO gaps calculated from computational studies, electrochemical measurements (the difference between the oxidation and reduction potentials) and lowest-energy absorption band maxima are listed in Table 2. The calculated band gaps from DFT and UV–visible spectral bands are in good agreement, displaying almost same energy gaps for compounds **2**–**5**. The little differences in band gaps from DFT and UV–visible spectral bands are associated with the interactive mediums, where solvent contributions on the band gaps have been neglected in theoretical calculations. The band gaps obtained from electrochemical measurements are relatively smaller than the values obtained from DFT and UV–visible spectral bands.[17] However, the electrochemically measured band gaps for **2**–**6** are, on an average, same and within experimental error limit (±5%). For **2**–**6**, the HOMO is localized in the peripheral donor arms with some degree of orbital coefficient on pyrene core, whereas LUMO is located mainly on peripheral acceptor arms with some degree of orbital coefficient on pyrene core (Fig. S1).

Therefore, it is expected that probable intramolecular charge transfer (ICT) occurs from peripheral donor arms to peripheral acceptor arms through pyrene core (D-π-cA-π-A). We have theoretically studied spin density distribution in radical cations/anions of **1**–**6** to understand the radical stability at the molecular level. We have considered the net spin, which leads to a difference between the electron densities for the spin up (alpha) and spin down (beta) states. Fig. 3 gives the spin density isosurfaces of singly occupied molecular orbitals (SOMO) of cations and anions for compounds **1**–**6**. In the case of cation radicals SOMOs correspond to their HOMOs (Fig. S1, Supplementary data). As shown in Fig. 3, the net spin density in the SOMOs of **2**–**5** resides on the pyrene core as well as on the donor arms and the density delocalization[18] occurs with increasing number of donor groups (**2**→**6**). This overall electron spin density delocalization in the SOMO surfaces supports the enhanced cation radical stability in going from **2** to **6**, because electron-deficient cation radical produced after oxidation needs immediate electron density to be thermodynamically stable and that can be supplied from other electron-rich peripheral donor arms. It can also be supported form calculated electrostatic potential (ESP) density distribution. The electrostatic potential density surfaces of the neutral molecule (centre), cation (left), anion (right) of compound **2** have been shown in Fig. 4. In Fig. 4, it is evident that positive charge (blue) of cation radicals resides mostly on donor arms along with pyrene core, whereas negative charge (red) of anion radicals resides mostly on acceptor arms along with pyrene core, implying that positive charge distribution in cation radicals depends on number of donor arms and negative charge distribution in anion radicals depends on number of acceptor arms. It is interesting to notice that although **3** and **4** have same number of donor groups, the cation radical produced from **3** is not so stable (i.e., the oxidation peak is not reversible, Fig. 2) whereas the cation radical produced from **4** is very stable. In the case of anion radicals SOMOs correspond to their LUMOs (Fig. S1, Supplementary data). The spin density of anion is located basically on the pyrene core and in acceptor arms. The pyrene core in **1**–**6** is known as electron-deficient moiety.[1,9a] Therefore, the pyrene core together with acceptor arms functionalized with electron withdrawing groups ($-CF_3$) will delocalize the excess electron density in the molecule after it is being reduced. Consequently, the anion radical stability increases with increasing number of acceptor groups (**6**→**2**). The anion radical produced after reduction in **6** is the least stable among **2**–**6** because there are no acceptor arms attached to pyrene core. The calculated non-adiabatic reduction (cation→neutral) potential (NRP)[9a] for the cation radicals of **1**–**6** are, respectively, −6.31, −5.83, −5.46, −5.45, −5.17, and −4.90 eV, which indicates that compounds with less number of peripheral donor groups (**1**–**4**) are more stable upon addition of one electron than the compounds with more number of peripheral donor groups (**5** and **6**). Conversely, cation radicals with more number of peripheral donor groups (**5** and **6**) are more stable than that with less number of peripheral donor groups (**1**–**4**), which are consistent with the analysis based on photophysical and electrochemical measurements. It is noted that cation radicals of **3** and **4** (with same number of peripheral donor groups), according to the calculated non-adiabatic reduction potential, have little difference in their stability. However, in cyclic voltammograms (Fig. 2), **3** and **4** have distinct differences in oxidation peak reversibility. On the other hand, the calculated vertical detachment energy (VDE)[9a] (anion→neutral) of anion radicals **1**–**6** are, respectively, 2.11, 1.84, 1.58, 1.58, 1.31, and 1.02 eV, which implies that anion radical stability increases on going from **6** to **1**, which are also consistent with our experimental observations.

To understand the differences between **3** and **4** in oxidation, we have calculated the molecular static first hyperpolarizability (β),[19] which can help to understand the geometry or electronic deformation of the molecules under external electronic perturbation. The details of static first hyperpolarizability tensor components for **3** and **4** are listed in Table S1 (Supplementary data). We could not check the experimental β values, as we did not get any single crystal for those compounds. However, we would find here the qualitative understanding about the cation radical stabilities of **3** and **4** from the calculated β values. The calculated total static first hyperpolarizability (β) of **3** is $\sim 56{,}515\times10^{-30}$ esu, which is ~974-fold larger than that of **4** (58×10^{-30} esu). The non-centrosymmetric geometry of **3** may be responsible for such large β value[20] in **3**. The large β in **3** suggests that electron density from the electron-rich region (NMe_2-funtionalized arms) can be highly deformed towards electron-deficient region ($-CF_3$ functionalized arms), which may reduce the stability of cation radicals produced electrochemically during oxidation process. This may be a possible reason for the less stability of cation radical of **3** compared to **4**. It is noteworthy that the hyperpolarizability effect becomes less significant in the present target molecules when the number of peripheral donor groups increases (or the number of peripheral acceptor groups decreases). On the contrary, we observed very little differences between **3** and **4** in the reduction region of the cyclic voltammograms. The reduction peaks for both the compounds are reversible. The peaks occur at almost same position, ~−1.78 V. The reasons may be the presence of central acceptor unit (pyrene moiety) along with the two peripheral acceptor groups in both the compounds, where central acceptor unit and two peripheral acceptor groups simultaneously can participate to stabilize the anion radicals, dominating over the effects of different substitution pattern of the acceptor groups in tetrakis(ethynyl)pyrenes.

3. Conclusions

We have synthesized a series of donor-pyrene-acceptor (**1**–**5**) by varying the substitution pattern and the number of functional groups in tetrakis(ethynyl)pyrenes, and performed their photophysical, electrochemical and computational studies. The redox potentials and radical stability of **2**–**5** have been compared with a standard ECL-active material of the similar kind (compound **6** in the present article) reported in Ref. 9a. From electrochemical reversibility, it is observed that cation radical stability enhances with the number of peripheral donor groups and anion radical stability enhances with the number of peripheral acceptor groups appended to tetrakis(ethynyl)pyrenes, while the total number of peripheral donor and acceptor groups is fixed (here the total number is 4). These experimental observations are also supported by theoretical calculations based on density functional theory (DFT). The net spin density is mainly located in peripheral donor arms along with pyrene core in case of cation radical, whereas it is located in peripheral acceptor arms along with pyrene core in case of anion radical, which implies that cation and anion radical stability at the molecular level depends, respectively, on number of peripheral donor and acceptor arms. The predicted radical stability at the molecular level from calculated non-adiabatic reduction potential (NRP) and vertical detachment energy (VDE), respectively, for cations and anions of **1**–**6** are also consistent with the experimental observations. In addition, differences in stability of cation radicals in oxidation process for the different substitution pattern (**3** and **4**) have been rationalized with the calculated static first hyperpolarizability (β). Therefore, we may conclude that electrochemical properties of the materials can be controlled by varying the number of functional groups, characteristics of functional groups (electron withdrawing or donating) and substitution patterns, which, in turn, may control the ECL efficiency of the materials. Studies of the ECL properties for these compounds would be interesting as **4** and **5** have a possibility of being stronger ECL materials compared to **6**.

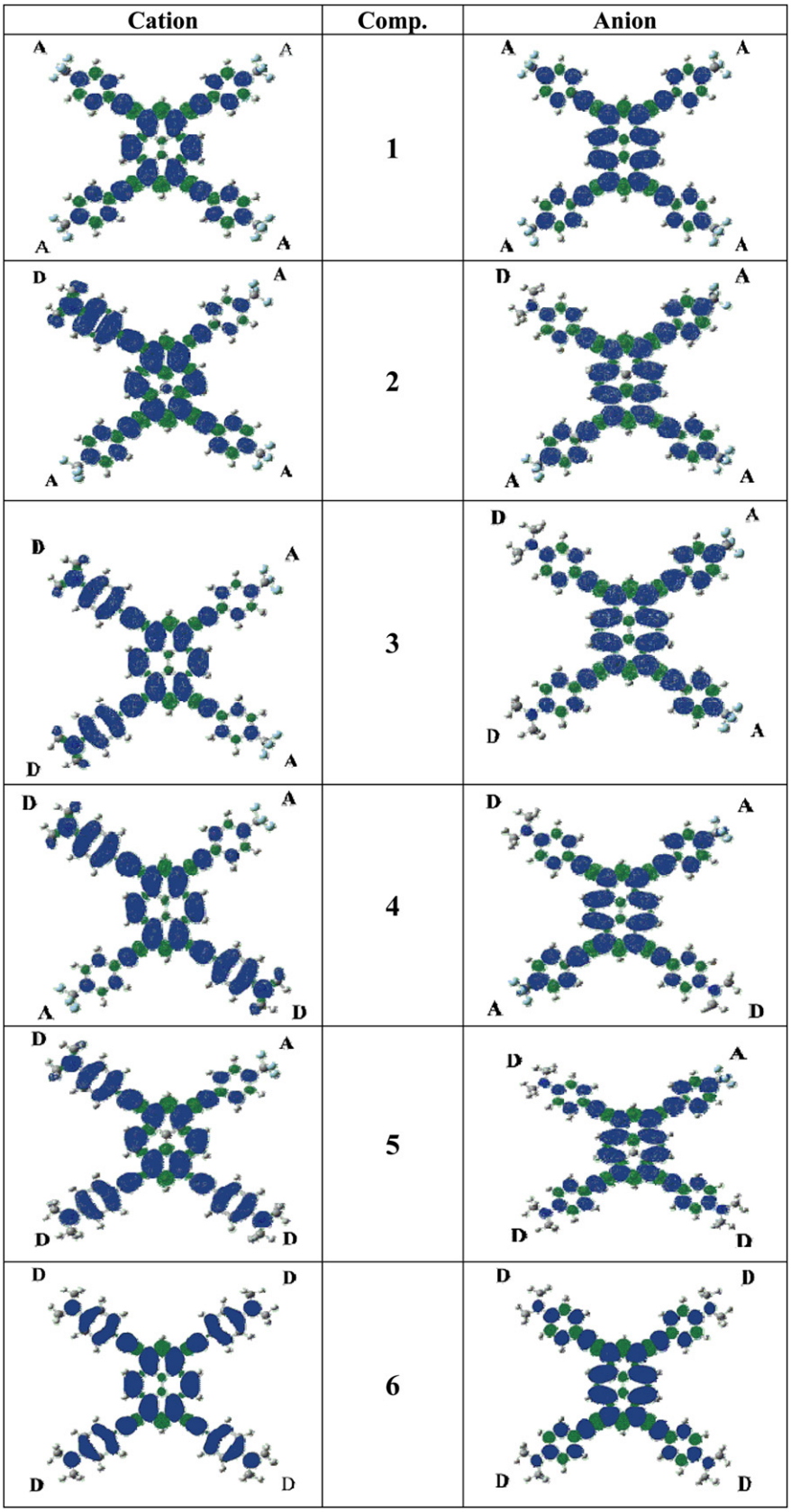

Fig. 3. The spin density isosurfaces (at a value of 0.0004 a.u.) of singly occupied molecular orbitals (SOMO) of cation and anion radicals for compounds **1**–**6**. Blue and green areas refer to regions of positive and negative spin density, respectively.

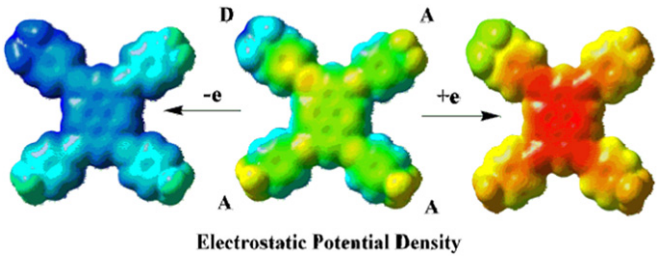

Fig. 4. The calculated electrostatic potential (ESP) density of **2** (middle), after removing one electron from **2** (left), and after adding one electron to **2** (right). The more blue and more red, respectively, indicate more positive and more negative electrostatic potentials. Isovalue of the isosurfaces is 0.0004 a.u.

4. Experimental section

4.1. Spectroscopic measurements

Absorption spectra were recorded on a Hewlett-Packard 8453 diode array spectrophotometer with 20 M solution of **1**–**6** in CH_2Cl_2 and photoluminescence spectra were obtained with Hitachi F-7000 fluorescence spectrometer with a 1 cm standard quartz cell using 3 M solution conditions in various solvents, respectively. The fluorescence quantum yields were determined by using Rhodamine 6G as the reference by the literature method.[15]

4.2. Electrochemistry measurements

Cyclic voltammetry (CV) was carried out using an electrochemical analyzer (CH Instruments 624C); 1 Hz stepwise potentials were generated for 20 s using a CHI 624C. Electrochemical experiments were referenced with respect to the Ag/AgCl reference electrode. All potentials were measured by the addition of ferrocene as an internal standard, where $E^o(Fc^+/Fc)$=70 mV versus Ag/AgCl. A platinum disk (2 mm diameter) working electrode was polished on a felt with 0.05 μM alumina (Buehler), rinsed with water and sonicated in absolute ethanol for 5 min. Then it was dried with Ar gas flow before each experiment. Dichloromethane solutions for CV measurement contained 0.5 mM tetrakis(ethynyl)pyrenes, respectively, and 0.1 M $TBAPF_6$ as an electrolyte.

4.3. Computational details

The geometries of compounds **1**–**6** and the geometries of their corresponding cation/anion radical species were optimized at B3LYP/6-31G(d) level of theory. The frontier molecular orbital energy and orbital surfaces, spin density distribution (SDD) surfaces, electrostatic potential (ESP) density surfaces, non-adiabatic reduction potential (NRP), vertical electron detachment energy (VDE) and static first hyperpolarizability (β) were also calculated at the same level of theory using optimized geometries. The non-adiabatic reduction potential (NRP) for cation radicals and vertical electron detachment energy (VDE) for anion radicals were calculated by using the following relation.[9a]

$$\text{NRP for cation radical} = E_c(\text{neutral}) - E_c(\text{cation}) \quad (1)$$

$$\text{VDE for anion radical} = E_a(\text{neutral}) - E_a(\text{anion}) \quad (2)$$

where, E_c (cation) and E_a (anion) are, respectively, energy of the cation and anion radical species. E_c (neutral) and E_a (neutral) represent the energy of the neutral system bearing, respectively, the optimized structure of the cation and anion radicals. The static first hyperpolarizability (β) was calculated analytically by density functional theory (DFT). The total static first hyperpolarizability (β_{tot}) was estimated by the following relations.[19]

$$\beta_{tot} = \left[(\beta_{xxx}+\beta_{xyy}+\beta_{xzz})^2 + (\beta_{yyy}+\beta_{yxx}+\beta_{yzz})^2 + (\beta_{zzz}+\beta_{zxx}+\beta_{zyy})^2\right]^{1/2} \quad (3)$$

The details of static first hyperpolarizability tensor components for **3** and **4** are listed in Table S1 (Supplementary data). The electronic excitation energies were calculated by using time-dependent density functional theory (TDDFT) at B3LYP/6-31G(d) level of theory. As we were interested only in qualitative results, we did not use any other diffuse functions in the basis set for calculating hyperpolarizability or electronic excitation energies. All calculations were performed using the Gaussian 09 W program package.[16]

4.4. 1-[(4-*N*,*N*-Dimethylaminophenyl)ethynyl]-3,6,8-tris[(4-trifluoromethylphenyl)ethynyl]pyrene (2)

Compound **7** (100 mg, 0.172 mmol), $PdCl_2(PPh_3)_2$ (21 mg, 0.03 mmol), CuI (12 mg, 0.063 mmol), PPh_3 (76 mg, 0.288 mmol), and 4-ethynyl-benzotrifluoride (116 mg, 0.688 mmol) were added to a degassed solution of triethylamine (40 ml) and toluene (60 ml) under Ar. The resulting mixture was stirred at 100 °C for 2 h. The solvent was removed under vacuum to give crude mixture. Compound **2** (32 mg) was obtained after column chromatography (silica gel, hexane/dichloromethane, 7:3, v/v). Mp 280–290 °C. IR (KBr pellet, cm^{-1}): 2200 (C≡C), 1609, 1522, 1359 (C–N), 1323. ^1H NMR (400 MHz, $CDCl_3$): δ 8.62 (d, J=9.4 Hz, 1H), 8.59–8.54 (m, 3H), 8.34 (d, J=3.8 Hz, 2H), 7.77 (d, J=7.9 Hz, 6H), 7.71 (d, J=8.3 Hz, 4H), 7.56 (d, J=8.8 Hz, 4H), 6.70 (d, J=9.2 Hz, 4H), 3.05 (s, 6H). ^{13}C NMR: spectrum could not be recorded due to inadequate solubility. HRMS: calcd 849.2078, found 849.2073.

4.5. 1,8-Bis[(4-*N*,*N*-dimethylaminophenyl)ethynyl]-3,6-bis[(4-trifluoromethylphenyl)ethynyl]pyrene (3)

Compound **8** (80 mg, 0.124 mmol), $PdCl_2(PPh_3)_2$ (20 mg, 0.028 mmol), CuI (11 mg, 0.058 mmol), PPh_3 (70 mg, 0.267 mmol), and 4-ethynyl-benzotrifluoride (105 mg, 0.62 mmol) were added to a degassed solution of triethylamine (40 ml) and toluene (60 ml) under Ar. The resulting mixture was stirred at 100 °C for 2 h. The solvent was removed under vacuum to give compound **3**. The crude product was then subjected to column chromatography (silica gel, hexane/dichloromethane, 7:3, v/v) to yield **3** (55 mg) as a red powder. Mp 271–280 °C. IR (KBr pellet, cm^{-1}): 2194 (C≡C), 1606, 1522, 1358 (C–N), 1320. ^1H NMR (300 MHz, $CDCl_3$): δ 8.65 (s, 2H), 8.51 (s, 2H), 8.31 (s, 2H), 7.77 (d, J=7.7 Hz, 4H), 7.64 (d, J=8.3 Hz, 4H), 7.58 (d, J=8.9 Hz, 4H), 6.72 (d, J=8.3 Hz, 4H), 3.05 (s, 12H). ^{13}C NMR: spectrum could not be recorded due to inadequate solubility. HRMS: calcd 824.2626, found 824.2626.

4.6. 1,6-Bis[(4-*N*,*N*-dimethylaminophenyl)ethynyl]-3,8-bis[(4-trifluoromethylphenyl)ethynyl]pyrene (4)

Compound **9** (30 mg, 0.046 mmol), $PdCl_2(PPh_3)_2$ (10 mg, 0.014 mmol), CuI (6 mg, 0.032 mmol), PPh_3 (25 mg, 0.095 mmol), and 4-ethynyl-benzotrifluoride (40 mg, 0.24 mmol) were added to a degassed solution of triethylamine (15 ml) and toluene (30 ml) under Ar. After stirring at 100 °C for 2 h, the red precipitate was filtered and washed with toluene and then recrystallization from $CHCl_3$ to afford the pure desired compound as a red powder (38 mg). Mp >300 °C. IR (KBr pellet, cm^{-1}): 2191

(C≡C), 1606, 1522, 1362 (C–N), 1323. ^{1}H NMR (300 MHz, $CDCl_3$): δ 8.75 (d, J=9.6 Hz, 2H), 8.68 (d, J=8.9 Hz, 2H), 8.41 (s, 2H), 7.82 (d, J=7.9 Hz, 4H), 7.70 (d, J=7.9 Hz, 4H), 7.60 (d, J=8.3 Hz, 4H), 6.70 (d, J=8.9 Hz, 4H), 3.06 (s, 8H). ^{13}C NMR: spectrum could not be recorded due to inadequate solubility. HRMS: calcd 824.2626, found 824.2631.

4.7. 1,3,6-Tris[(4-*N*,*N*-dimethylaminophenyl)ethynyl]-8-[(4-trifluoromethylphenyl)ethynyl]pyrene (5)

Compound **10** (250 mg, 0.352 mmol), $PdCl_2(PPh_3)_2$ (20 mg, 0.03 mmol), CuI (13 mg, 0.071 mmol), PPh_3 (77 mg, 0.290 mmol), and 4-ethynyl-trifluoromethyl benzene (120 mg, 0.710 mmol) are added to a degassed solution of triethylamine (50 ml) and toluene (100 ml) under Ar. The resulting mixture was heated at 100 °C with stirring for 2 h. After the mixture was cooled, the red precipitate was filtered and washed with toluene and then recrystallized from $CHCl_3$ to afford the pure desired compound as a red powder (232 mg). Mp >300 °C. IR (KBr pellet, cm^{-1}): 2191 (C≡C), 1607, 1528, 1362 (C–N), 1318. ^{1}H NMR (400 MHz, $CDCl_3$): δ 8.71 (q, J=8.0 Hz, 3H), 8.61 (d, J=9.2 Hz, 1H), 8.35 (d, J=3.9 Hz, 2H), 7.82 (d, J=8.2 Hz, 4H), 7.69 (d, J=8.9 Hz, 4H), 7.60 (d, J=7.9 Hz, 6H), 6.73 (d, J=8.2 Hz, 6H), 3.06 (s, 18H). ^{13}C NMR: spectrum could not be recorded due to inadequate solubility. HRMS: calcd 799.3174, found 799.3175.

4.8. Compounds 7–10

1,3,6,8,-Tetrabromopyrene (10.0 g, 19.3 mmol), $PdCl_2(PPh_3)_2$ (100 mg, 0.142 mmol), CuI (27 mg, 0.142 mmol), PPh_3 (75 mg, 0.286 mmol), and 4-ethynyl-*N*,*N*-dimethylaniline (1 g, 6.89 mmol) were added to a degassed solution of triethylamine (200 ml) and toluene (350 ml) under Ar. The resulting mixture was stirred at 100 °C for 2 h. The solvent was removed under vacuum to give a mixture of compounds **7**–**10**. Compounds **7** (201 mg, yellow solid), **8** (189 mg, yellow orange solid), **9** (38 mg, yellow orange solid) and **10** (335 mg, red orange solid) were separated by column chromatography (silica gel, hexane/dichloromethane, 7:3, v/v).

*4.8.1. 1,6,8-Tribromo-3-[4-(N,N-dimethylamino)phenylethynyl]pyrene (**7**).* Mp 252–260 °C. IR (KBr pellet, cm^{-1}): 2185 (C≡C), 1591, 1524, 1363 (C–N), 1062. ^{1}H NMR (300 MHz, $CDCl_3$): δ 8.75 (d, J=8.9 Hz, 1H), 8.56–8.43 (m, 5H), 7.60 (d, J=8.5 Hz, 2H), 6.74 (d, J=8.6 Hz, 2H), 3.06 (s, 6H). ^{13}C NMR: spectrum could not be recorded due to inadequate solubility. HRMS: calcd 578.8833, found 578.8833.

*4.8.2. 1,8-Dibromo-3,6-bis[4-(N,N-dimethylamino)phenylethynyl]pyrene (**8**).* Mp >300 °C. IR (KBr pellet, cm^{-1}): 2185 (C≡C), 1606, 1522, 1358 (C–N), 1166. ^{1}H NMR (300 MHz, $CDCl_3$): δ 8.71 (s, 2H), 8.45 (d, J=9.6 Hz, 4H), 7.61 (d, J=8.9 Hz, 4H), 6.73 (d, J=8.6 Hz, 4H), 3.05 (s, 12H). ^{13}C NMR (100 MHz, $CDCl_3$): δ 156.7, 133.8, 133.2, 131.2, 129.7, 127.7, 126.6, 125.2, 121.2, 120.2, 112.1, 109.8, 98.9, 85.7, 40.4. HRMS: calcd 646.0463, found 646.0439.

*4.8.3. 1,6-Dibromo-3,8-bis[4-(N,N-dimethylamino)phenylethynyl]pyrene (**9**).* Mp >300 °C. IR (KBr pellet, cm^{-1}): 2190 (C≡C), 1606, 1523, 1369 (C–N), 1197. ^{1}H NMR (400 MHz, $CDCl_3$): δ 8.71 (d, J=9.8 Hz, 2H), 8.50 (d, J=9.3 Hz, 2H), 8.45 (s, 2H), 7.58 (d, J=9.1 Hz, 4H), 6.74 (d, J=8.9 Hz, 4H), 3.05 (s, 12H). ^{13}C NMR: spectrum could not be recorded due to inadequate solubility. HRMS: calcd 644.0463, found 647.0463.

*4.8.4. 1-Bromo-3,6,8-tris[4-(N,N-dimethylamino)phenylethynyl]pyrene (**10**).* Mp >300 °C. IR (KBr pellet, cm^{-1}): 2189 (C≡C), 1608, 1525, 1362 (C–N), 1197. ^{1}H NMR (300 MHz, $CDCl_3$): δ 8.69 (q, J=9.0 Hz, 3H), 8.44 (d, J=9.4 Hz, 1H), 8.38 (d, J=12.9 Hz, 2H), 7.59 (d, J=8.8 Hz, 6H), 6.73 (d, J=8.7 Hz, 6H), 3.06 (s, 18H). ^{13}C NMR (100 MHz, $CDCl_3$): δ 150.58, 150.51, 133.44, 133.32, 133.21, 133.17, 131.16, 131.35, 131.04, 130.64, 127.59, 126.66, 125.57, 124.23, 120.56, 120.15, 120.01, 119.94, 112.11, 112.08, 110.21, 110.15, 109.92, 98.50, 97.78, 97.72, 86.39, 86.29, 85.95, 40.46, 40.45, HRMS: calcd 709.2093, found 710.2069.

Acknowledgements

This work was supported by Sookmyung Women's University Research Grant 2009.

Supplementary data

Supplementary data related to this article can be found online at doi:10.1016/j.tet.2011.12.066.

References and notes

1. (a) Figueira-Duarte, T. M.; Müllen, K. *Chem. Rev.* **2011**, *111*, 7260–7314; (b) Watson, M. D.; Fechtenkötter, A.; Müllen, K. *Chem. Rev.* **2001**, *101*, 1267–1300.
2. (a) Jiang, J. X.; Xu, Y. H.; Yang, W.; Guan, R.; Liu, Z. Q.; Zhen, H. Y.; Cao, Y. *Adv. Mater.* **2006**, *18*, 1769–1773; (b) Liu, J.; Zhou, Q. G.; Cheng, Y. X.; Geng, Y. H.; Wang, L. X.; Ma, D. G.; Jing, X. B.; Wang, F. S. *Adv. Mater.* **2005**, *17*, 2974–2978; (c) Gong, X.; Wang, S.; Moses, D.; Bazan, G. C.; Heeger, A. J. *Adv. Mater.* **2005**, *17*, 2053–2058; (d) Qiu, Y.; Wei, P.; Zhang, D. Q.; Qiao, J.; Duan, L.; Li, Y. K.; Gao, Y. D.; Wang, L. D. *Adv. Mater.* **2006**, *18*, 1607–1611; (e) Shao, Y.; Yang, Y. *Appl. Phys. Lett.* **2005**, *86*, 073510(1)–073510(3); (f) Carlson, B.; Phelan, G. D.; Kaminsky, W.; Dalton, L.; Jiang, X. Z.; Liu, S.; Jen, A. K. Y. *J. Am. Chem. Soc.* **2002**, *124*, 14162–14172.
3. (a) Goedeweeck, R.; Vanderauweraer, M.; Deschryver, F. C. *J. Am. Chem. Soc.* **1985**, *107*, 2334–2341; (b) Hammarstrom, P.; Kalman, P. B.; Jonsson, B. H.; Carlsson, U. *FEBS Lett.* **1997**, *420*, 63–68; (c) Sahoo, D.; Weers, P. M. M.; Ryan, R. O.; Narayanaswami, V. *J. Mol. Biol.* **2002**, *321*, 201–214; (d) Sahoo, D.; Narayanaswami, V.; Kay, C. M.; Ryan, R. O. *Biochemistry* **2000**, *39*, 6594–6601.
4. (a) Paris, P. L.; Langenhan, J. M.; Kool, E. T. *Nucleic Acids Res.* **1998**, *26*, 3789–3793; (b) Lewis, F. D.; Zhang, Y. F.; Letsinger, R. L. *J. Am. Chem. Soc.* **1997**, *119*, 5451–5452; (c) Yamana, K.; Iwai, T.; Ohtani, Y.; Sato, S.; Nakamura, M.; Nakano, H. *Bioconjugate Chem.* **2002**, *13*, 1266–1273; (d) Tong, G.; Lawlor, J. M.; Tregear, G. W.; Haralambidis, J. *J. Am. Chem. Soc.* **1995**, *117*, 12151–12158.
5. (a) Ollmann, M.; Schwarzmann, G.; Sandhoff, K.; Galla, H. J. *Biochemistry* **1987**, *26*, 5943–5952; (b) Pap, E. H. W.; Hanicak, A.; van Hoek, K. W. A.; Wirtz, A. J. W.; Visser, G. *Biochemistry* **1995**, *34*, 9118–9125; (c) Somerharju, P. *Chem. Phys. Lipids* **2002**, *116*, 57–74.
6. Tang, C. W. *Appl. Phys. Lett.* **1986**, *48*, 183–185.
7. (a) Chabinyc, M. L.; Salleo, A. *Chem. Mater.* **2004**, *16*, 4509–4521; (b) Veres, J.; Ogier, S.; Lloyd, G.; de Leeuw, D. *Chem. Mater.* **2004**, *16*, 4543–4555; (c) McCulloch, I.; Heeney, M.; Bailey, C.; Genevicius, K.; MacDonald, I.; Shkunov, M.; Sparrowe, D.; Tierney, S.; Wagner, R.; Zhang, W. M.; Chabinyc, M. L.; Kline, R. J.; McGehee, M. D.; Toney, M. F. *Nat. Mater.* **2006**, *5*, 328–333; (d) Allard, S.; Forster, M.; Souharce, B.; Thiem, H.; Scherf, U. *Angew. Chem., Int. Ed.* **2008**, *47*, 4070–4098.
8. (a) Marsden, J. A.; Miller, J. J.; Shirtcliff, L. D.; Haley, M. M. *J. Am. Chem. Soc.* **2005**, *127*, 2464–2476; (b) Spitler, E. L.; Shirtchliff, L. D.; Haley, M. M. *J. Org. Chem.* **2007**, *72*, 86–96; (c) Zucchero, A. J.; Wilson, J. N.; Bunz, U. H. F. *J. Am. Chem. Soc.* **2006**, *128*, 11872–11881.
9. (a) Oh, J.-W.; Lee, Y. O.; Kim, T. H.; Ko, K. C.; Lee, J. Y.; Kim, H.; Kim, J. S. *Angew. Chem., Int. Ed.* **2009**, *48*, 2522–2524; (b) Fujimato, K.; Shimizu, H.; Furusuyo, M.; Akiyama, S.; Ishida, M.; Furukawa, U.; Yokoo, T.; Inouye, M. *Tetrahedron* **2009**, *65*, 9357–9361.
10. (a) Rashidnadimi, S.; Hung, T. H.; Wong, K.-T.; Bard, A. J. *J. Am. Chem. Soc.* **2008**, *130*, 634–639; (b) Jiang, X.; Yang, X.; Zhao, C.; Jin, K.; Sun, L. *J. Phys. Chem. C* **2007**, *111*, 9595–9602.
11. (a) Yang, M.; Jacquemin, D.; Champagne, B. *Phys. Chem. Chem. Phys.* **2002**, *4*, 5566–5571; (b) Richter, M. M. *Chem. Rev.* **2004**, *104*, 3003–3036; (c) Miao, W. *Chem. Rev.* **2008**, *108*, 2506–2553; (d) Grimsdale, A. C.; Chan, K. L.; Martin, R. E.; Jokisz, P. G.; Holmes, A. B. *Chem. Rev.* **2009**, *109*, 897–1091.
12. Yang, J.-S.; Liau, K.-L.; Wang, C.-M.; Hwang, C.-Y. *J. Am. Chem. Soc.* **2004**, *126*, 12325–12335.
13. (a) Maeda, H.; Maeda, T.; Mizuno, K.; Fujimoto, K.; Shimizu, H.; Inouye, M. *Chem.—Eur. J.* **2006**, *12*, 824–831; (b) Venkataramana, G.; Sankararaman, S. *Eur. J. Org. Chem.* **2005**, 4162–4166; (c) Yang, S.-W.; Elangovan, A.; Hwang, K.-C.; Ho, T.-I. *J. Phys. Chem. B* **2005**, *109*, 16628–16635; (d) Shimizu, H.; Fujimoto, K.; Furusyo, M.; Maeda, H.; Nanai, Y.; Mizuno, K.; Inouye, M. *J. Org. Chem.* **2007**, *72*, 1530–1533; (e) Long, N. J.; Williams, C. K. *Angew. Chem., Int. Ed.* **2003**, *42*, 2586–2617; (f) Kim, H. M.; Lee, Y. O.; Lim, C. S.; Kim, J. S.; Cho, B. R. *J. Org. Chem.* **2008**, *73*, 5127–5130.
14. Wang, S.; Cai, J.; Sadygov, R.; Lim, E. C. *J. Phys. Chem.* **1995**, *99*, 7416–7420.
15. Crosby, G. A.; Demas, J. N. *J. Phys. Chem.* **1971**, *75*, 991–1024.

16. Frisch, M. J.; Trucks, G. W.; Schlegel, H. B.; Scuseria, G. E.; Robb, M. A.; Cheeseman, J. R.; Scalmani, G.; Barone, V.; Mennucci, B.; Petersson, G. A.; Nakatsuji, H.; Caricato, M.; Li, X.; Hratchian, H. P.; Izmaylov, A. F.; Bloino, J.; Zheng, G.; Sonnenberg, J. L.; Hada, M.; Ehara, M.; Toyota, K.; Fukuda, R.; Hasegawa, J.; Ishida, M.; Nakajima, T.; Honda, Y.; Kitao, O.; Nakai, H.; Vreven, T.; Montgomery, J. A., Jr.; Peralta, J. E.; Ogliaro, F.; Bearpark, M.; Heyd, J. J.; Brothers, E.; Kudin, K. N.; Staroverov, V. N.; Keith, T.; Kobayashi, R.; Normand, J.; Raghavachari, K.; Rendell, A.; Burant, J. C.; Iyengar, S. S.; Tomasi, J.; Cossi, M.; Rega, N.; Millam, J. M.; Klene, M.; Knox, J. E.; Cross, J. B.; Bakken, V.; Adamo, C.; Jaramillo, J.; Gomperts, R.; Stratmann, R. E.; Yazyev, O.; Austin, A. J.; Cammi, R.; Pomelli, C.; Ochterski, J. W.; Martin, R. L.; Morokuma, K.; Zakrzewski, V. G.; Voth, G. A.; Salvador, P.; Dannenberg, J. J.; Dapprich, S.; Daniels, A. D.; Farkas, O.; Foresman, J. B.; Ortiz, J. V.; Cioslowski, J.; Fox, D. J. *Gaussian 09, Revision B.01*; Gaussian: Wallingford, CT, 2010.
17. Lin, J. H.; Elangovan, A.; Ho, T.-I. *J. Org. Chem.* **2005**, *70*, 7397–7407.
18. (a) Baumgarten, M.; Koch, K.-H.; Müllen, K. *J. Am. Chem. Soc.* **1994**, *116*, 7341–7348; (b) Palacio, F.; Anntorena, G.; Castro, M.; Burriel, R.; Rawson, J. M.; Smith, J. N. B.; Bricklebank, N.; Novoa, J.; Ritter, C. *Phys. Rev. Lett.* **1997**, *79*, 2336–2339; (c) Veciana, J. In *Molecular Magnetism: From Molecular Assemblies to the Devices*; Coronado, E., Delhaes, P., Gatteschi, D., Miller, J. S., Eds.; NATO ASI Series; Kluwer Acad.: Dordrecht, 1996; Vol. 321, p 425.
19. (a) Hinchliffe, A.; Machado, H. J. S. *Int. J. Mol. Sci.* **2000**, *1*, 39–48; (b) Meyers, F.; Bredas, J. L.; Zyss, J. *J. Am. Chem. Soc.* **1992**, *114*, 2914–2921; (c) Isborn, C. M.; Leclercq, A.; Vila, F. D.; Dalton, L. R.; Brédas, J. L.; Eichinger, B. E.; Robinson, B. H. *J. Phys. Chem. A* **2007**, *111*, 1319–1327.
20. Cardoso, C.; Abreu, P. E.; Nogueira, F. *J. Chem. Theory Comput.* **2009**, *5*, 850–852.